Advanced Functional Materials

ADVANCED FUNCTIONAL MATERIALS
www.afm-journal.de

RESEARCH ARTICLE OPEN ACCESS

From Waste to Value: Conversion of Calcium Sulfate to Vaterite via Carbon Capture and Storage

Carlos Pimentel[1] | German Montes-Hernández[1] | Pablo Almarza-Cifuentes[2] | Matthias Kellermeier[3] | Alexander E.S. Van Driessche[1,2]

[1]Univ. Grenoble Alpes, Univ. Savoie Mont Blanc, CNRS, IRD, IFSTTAR, ISTerre, Grenoble, France | [2]IACT-CSIC, Avenida delas Armilla, Granada, Spain | [3]Material Science, BASFSE, Ludwigshafen, Germany

Correspondence: Carlos Pimentel (cpimentelguerra@geo.ucm.es) | Matthias Kellermeier (matthias.kellermeier@basf.com) | Alexander E.S. Van Driessche (alexander.vd@csic.es)

Received: 31 July 2025 | **Revised:** 9 December 2025 | **Accepted:** 8 January 2026

Keywords: calcium carbonate | calcium sulfate | carbon capture storage and utilization | mineralization | polymorphism | Raman spectroscopy | vaterite

ABSTRACT

Developing effective solutions to reduce carbon dioxide emissions into the atmosphere is crucial for mitigating climate change. While various methods for CO_2 capture and storage exist, many of the proposed approaches are not yet economically viable on larger scales. Here we introduce a new sustainable strategy for carbon management that relies on the carbonation of calcium sulfate, an abundant byproduct of various industrial processes. Through in-situ observation tools, we uncover the carbonation mechanism and demonstrate that phase-pure vaterite (a metastable form of calcium carbonate) can be obtained without additives via straightforward conversion of gypsum powder in water at ambient conditions. The resulting particles exhibit interesting properties such as high specific surface area and reactivity. To demonstrate the value of the products for real-life applications, the obtained vaterite was tested as a raw material for construction. Upon mixing with water, the spherical vaterite particles transformed into aragonite crystals through a dissolution-reprecipitation pathway, which was accompanied by rapid compressive strength development on a level comparable to that of conventional cements. Our findings constitute an important first step toward repurposing gypsum waste as a sink for carbon dioxide and source to produce materials with reduced environmental impact.

1 | Introduction

Since the onset of the industrial revolution, carbon dioxide emissions into the Earth's atmosphere from fossil fuel utilization and numerous industrial processes have continuously risen and reached 37 Gt per year in 2022 [1]. Identified as a primary driver of contemporary climate change, [2] efforts have been made to reduce these emissions, for example by the use of renewable energy sources and the transformation of established industrial processes into more sustainable operations. Despite these initiatives, it is anticipated that anthropogenic CO_2 emissions will continue to escalate over the next 50 to 100 years [3]. Consequently, there is an immediate need for effective solutions to contain the release of carbon dioxide into the atmosphere. Over the past years, various methodologies have been proposed for carbon capture storage (CCS) and/or utilization (CCU) [4–8]. Concepts for the (permanent) storage of CO_2 can be classified into two main categories: deposition into geological sites in neat form or mineralization as carbonate. While geological storage is currently about four times cheaper than mineralization, the potential for leakage poses a significant concern and must be considered as another cost factor in addition to the required infrastructure [5]. In both cases, utilization of the captured carbon dioxide to produce industrially valuable compounds (e.g., green methanol for chemical synthesis or carbonate minerals as raw materials for construction) would not only be an important

contribution to lower the costs but also align with the principles of a circular economy [9].

The most common material obtained from CO_2 mineralization is calcium carbonate, typically in the form of one its anhydrous crystalline polymorphs, i.e., calcite, aragonite, or vaterite. These minerals are widely used in the production of paper, cosmetics and pharmaceuticals [10, 11] as well as in the construction industry [12]. While calcite and aragonite are abundant in the Earth's crust, vaterite is relatively rare in Nature but preferred for certain applications due to its high specific surface area and unique morphology [13]. However, the synthesis of phase-pure vaterite remains a challenging task. Methods described in the literature include rapid mixing, [14–16] slow carbonation, [17] CO_2 injection, [18, 19] solvothermal growth, [20] crystallization in reverse emulsions, [21, 22] and phase transfer precipitation [23]. Most of these approaches rely on the use of organic additives such as proteins, [24] ethanol, [19, 25, 26] ammonium ions, [14, 16, 19, 27] glycerol, [11, 20] or sodium gluconate [23]. Additive-free synthesis of vaterite was achieved by mixing highly concentrated solutions of $CaCl_2$ and Na_2CO_3 [10, 28, 29].

The conversion of CO_2 into $CaCO_3$ obviously requires a tangible source of calcium. Here, the use of waste materials appears particularly attractive from both a cost and sustainability perspective. In this context, calcium sulfate is a very interesting material, given the large amounts available from construction waste (e.g., spent wallboards) and as a byproduct of various industrial processes. Several previous studies have explored the potential of gypsum ($CaSO_4 \cdot 2H_2O$) as a calcium source for CO_2 mineralization [6, 30–32]. In some cases, vaterite was obtained as a product of carbonation under the influence of additives [18, 19, 23, 33, 34]. In the present work, we have systematically studied the carbonation of the three main calcium sulfate phases, i.e., gypsum, bassanite ($CaSO_4 \cdot 0.5H_2O$) and anhydrite (anhydrous $CaSO_4$) at ambient conditions in the absence of any additive. Using advanced in- situ characterization techniques (such as Raman spectroscopy and potentiometry), we uncover the carbonation mechanism and identify critical parameters required for the formation of phase-pure vaterite. Finally, we discuss the potential of the proposed process for carbon capture storage and utilization, gypsum waste management, and circular economy.

2 | Materials and Methods

2.1 | Materials

The following chemicals were used as received: gypsum (C3771, Sigma–Aldrich), bassanite (38 535 500, Acros Organics), anhydrite (237 132, Sigma–Aldrich), sodium carbonate (S2127, Sigma–Aldrich), potassium carbonate (P743.2, Sigma–Aldrich), sodium hydroxide (S5881, Sigma–Aldrich), potassium hydroxide (P1767, Sigma–Aldrich, >85%), magnesium chloride (Scharlau, 100%), strontium chloride (Thermo Scientific Chemicals, 99.5%) and carbon dioxide (UN1013, Messer). In addition, natural gypsum rock was obtained from Champ-sur-Drac (Isere, France) and identified with X-ray diffraction (PDF 33-0311). All solutions were prepared using deionized water with a resistivity of 18 MΩ·cm. To simulate the use of CO_2 emissions for the carbonation of calcium sulfate, two so-called "Alkaline Carbon Capture Solutions" (ACCS) were generated by bubbling solutions of 4 M NaOH (ACCS-Na) and KOH (ACCS-K) with CO_2 for 24 h, following a procedure described in the literature [35]. The composition and pH of the resulting solutions are provided in Table 1.

TABLE 1 | Solutions used for carbonation experiments in the present work.

	pH	Cation	Total carbonate concentration [M]
Na_2CO_3	11.7	Na	0.5
K_2CO_3	11.9	K	0.5
ACCS-Na	9.4–9.7	Na	~2.2
ACCS-K	9.4–9.7	K	~2.2

2.2 | Carbonation Experiments with In-Situ Monitoring by Raman Spectroscopy

The carbonation of sulfate minerals was performed at room temperature in two different setups. First, an autoclave reactor (0.6 L) equipped with a mechanical stirrer and a Raman probe with a 785 nm infrared laser was used. A comprehensive description of this custom-built equipment can be found in Montes-Hernandez and Renard [36]. The reactor was filled with ACCS or, for comparison, solutions of 0.5 M Na_2CO_3 or K_2CO_3 (200 mL). After initial characterization by Raman spectroscopy, 11 g solid calcium sulfate powder was added, giving nominal sulfate concentrations of 0.319, 0.379 and 0.404 M for gypsum, bassanite and anhydrite, respectively. Then, the reactor was sealed and stirring at 400 rpm was started. Raman spectra were acquired continuously until no more changes were observed. In the case of bassanite as calcium source, the early stages of the carbonation reaction were additionally characterized by means of time-resolved Fourier-transform infrared (FTIR) spectroscopy in attenuated total reflectance (ATR) mode, using a Bruker Tensor II spectrometer. For measurement, aliquots of the reaction solution were collected at various time intervals, and their infrared spectra were recorded. In separate experiments, the reaction was stopped after 2 and 80 min by isolation of the solid phase through vacuum filtration. The recovered products were characterized by FTIR spectroscopy in transmission mode on a Perkin Elmer SpectrumOne instrument as well as scanning electron microscopy (SEM) coupled with energy-dispersive X-ray (EDX) analysis using a Tescan Ambar X microscope equipped with an ULTIM MAX 100 detector from Oxford Instruments.

In the second part of the work, the experiments were replicated in a vessel equipped with sensors to monitor pH (Metrohm, No. 6.0262.100), Ca^{2+} potential by means of an ion-selective electrode (ISE; Metrohm, No. 6.0510.100), and conductivity using a 5-ring measuring cell (Metrohm, No. 6.0915.100), which were operated by a Titrando 905 unit from Metrohm. Again, 200 mL of the respective solution and 11 g of calcium sulfate powder were added and the resulting suspension was continuously stirred at 400 rpm.

Finally, some experiments were replicated in polypropylene bottles (50 mL) to prepare samples for ex- situ characterization, using 20 mL solution and 1.1 g calcium sulfate powder.

2.3 | Quantitative Evaluation of Raman Data

The spectra obtained from in-situ Raman spectroscopy monitoring were used to determine the time-dependent evolution of the concentrations of dissolved sulfate, carbonate and bicarbonate ions as well as the amounts of solid vaterite and calcite present in the suspension (note that aragonite was not detected in any of the experiments performed). For this purpose, calibration curves were generated by measuring Raman spectra of solutions containing the relevant ions in concentrations ranging from 0.005 to 1 M. Linear regressions were then applied to the data to correlate the intensity of the Raman peaks of the aqueous phases with the respective ion concentration. The relative amounts of vaterite and calcite formed during the carbonation reaction were determined using the equation proposed by Kontoyannis and Vagenas [37]:

$$X_V = \frac{9.3I_{750V}}{I_{711C} + 9.3I_{750V}} \times 100 \quad (1)$$

where X_V and X_C are, respectively, the fractions of vaterite and calcite in % (with $X_C = 100 - X_V$), while I_{750V} and I_{711C} are the intensities of the peaks at 750 cm^{-1} (vaterite) and 711 cm^{-1} (calcite), respectively. To obtain precise results, the measured intensity of the vaterite peak at 750 cm^{-1} was corrected for scattering contributions from the used sapphire window, which was determined during the first 4 min of the reaction and remained constant throughout the experiment.

2.4 | Characterization of Solid Products

For ex-situ characterization of the formed particles, the suspensions were vacuum-filtered through 0.45 µm nylon membranes, then washed with deionized water, and finally rinsed with ethanol to prevent any further reaction. Mineral phases present in the products were routinely identified by ATR-FTIR on a Nicolet iS50 spectrometer from Thermo Scientific and quantified with powder X-ray diffraction (PXRD) on a Bruker Axs D8 instrument equipped with Cu and Co sources. The relative amounts of vaterite and calcite were determined from the PXRD data using the equation proposed by Kontoyannis and Vagenas [37]:

$$X_V = \frac{7.691I_{11.0V}}{I_{10.4C} + 7.691I_{11.0V}} \times 100 \quad (2)$$

where X_V and X_C are, respectively, the fractions of vaterite and calcite in % (with $X_C = 100 - X_V$), while $I_{11.0V}$ and $I_{10.4C}$ are the intensities of the (11.0) and (10.4) reflections of vaterite and calcite, respectively.

The size and morphology of the formed particles were characterized by field-emission scanning electron microscopy (FESEM) on a Gemini SEM 500 microscope from Zeiss. Images were acquired with an aperture size of 20 µm, a working distance of 4.8 mm, and an accelerating voltage of 3 kV. For sample preparation, 10 mg solid product was mixed with 10 mL ultrapure ethanol and placed in an ultrasonic bath for 5 min. Two drops of the resulting suspension were deposited onto aluminium sample holders and allowed to dry before being placed in the vacuum chamber of the microscope. In the obtained SEM images, vaterite particles were identified based on their distinct spherical or star-like morphologies, which were all composed of numerous nanoparticles with sizes <100 nm. Calcite crystals, when present, exhibited their characteristic rhombohedral shape. Sizes of vaterite particles and their constituent subunits were quantified using the FIJI software [38]. Finally, the specific surface area (S_{BET}) of the solid products was determined by nitrogen sorption using a BELSORP MAX instrument from Microtrac. Prior to analysis, samples were degassed at 50°C for 12 h This thermal treatment was reported to not alter the properties of calcium carbonate samples [39]. S_{BET} values were derived using the Brunauer-Emmett-Teller (BET) equation from data in a partial pressure regime of $0.06 \leq p/p_0 \leq 0.3$ with an adsorption cross-section of 16.2 $Å^2$ for molecular nitrogen.

2.5 | Preparation and Characterization of Vaterite-Based Cements

The vaterite material used for compressive strength testing was synthesized by mixing 700 mL K_2CO_3 solution (0.5 M) with 38.5 g gypsum powder. The resulting suspension was stirred at 500 rpm for 15 min. Subsequently, the solid phase was separated by filtration and thoroughly rinsed with ethanol to remove any residual reactants. The predominant presence of vaterite in the obtained solid product was confirmed by ATR-FTIR spectroscopy. To initiate polymorphic transformation into aragonite, the vaterite powder (8 g) was manually mixed in an agate mortar with a solution containing 0.1 M of $MgCl_2$ and/or $SrCl_2$ at a water-to-vaterite ratio of 0.5. The resulting flowable paste was cast into silicone molds to produce cubic specimens measuring 20 × 20 × 20 mm^3, which were cured for 24 h at 40 or 80°C and >95% relative humidity (RH). Subsequently, the (meanwhile solidified) cubes were demolded and submerged in a $MgCl_2/SrCl_2$ solution (0.1 M each) at 80°C. After further curing for either 24 or 48 h, the cubes were removed from the solution and dried in an oven at 100°C for 4 h. For comparison, reference cubes were prepared using commercially available Ordinary Portland Cement (OPC, COSMOS CEM II/L-B 32.5N), which was mixed with (i) a solution containing 0.1 M each of $MgCl_2$ and $SrCl_2$, and (ii) with deionized water, both at a water-to-cement ratio of 0.5. Curing conditions were the same as those applied for the vaterite samples. However, a larger amount (10 g) of the cement paste was needed to fill the molds. The compressive strength development of the as-prepared cubes was evaluated after curing periods of 24 and 48 h. Mechanical properties were investigated using a Universal Testing Machine (INSTRON, Model 68TM-30) equipped with a 30 kN load cell and 150 mm diameter compression plates. The tests were conducted at a constant compression speed of 1 mm/min. The obtained load-displacement data were analyzed following ASTM C109 (with the exception that rigid plates were used) to obtain compressive strength values. The vaterite and aragonite content of the as-prepared $CaCO_3$ cement was quantified via FTIR spectroscopy in transmission mode on a Perkin Elmer SpectrumOne instrument, utilizing a calibration curve derived from binary mixtures of

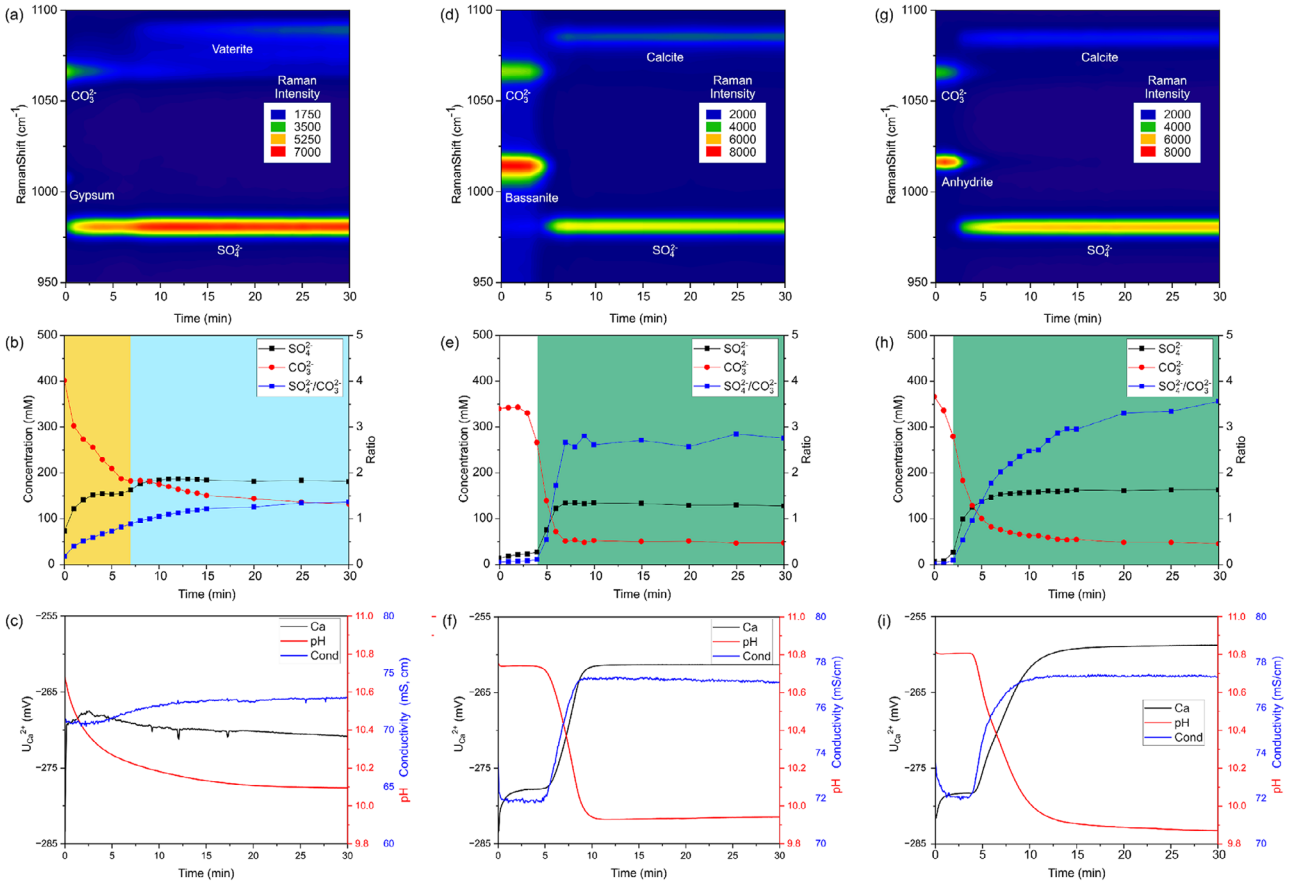

FIGURE 1 | In-situ monitoring of the carbonation of synthetic gypsum a–c), bassanite d–f) and anhydrite g–i) by reaction with a 0.5 M solution of sodium carbonate. a,d,g) 2D representation of time-dependent Raman spectra acquired during the carbonation process, where characteristic signals of the relevant solid phases and dissolved ions are monitored. b,e,h) Temporal evolution of the concentrations of dissolved sulfate and carbonate ions and their ratio, as derived from the in- situ Raman experiments. c,f,i) Plots of the calcium potential, pH and conductivity as a function of time during the carbonation reaction. In (b,e,h), the presence of ACC, vaterite and calcite is indicated by the yellow-, blue- and green-shaded rectangles, respectively.

known polymorphic content. The specific surface area of the materials was determined by nitrogen sorption using an ASAP 2420 micropore analyzer from Micromeritics after degassing in vacuum for 12 h at 50°C. Data were evaluated using the BET model for a partial pressure regime of $0.05 \leq p/p_0 \leq 0.2$. Finally, the microstructure of the hardened cement samples was characterized by scanning electron microscopy on a Phenom Pharos G2 tabletop microscope from ThermoFisher Scientific operated at an acceleration voltage of 10 kV.

3 | Results and Discussion

3.1 | Carbonation of Calcium Sulfate Minerals in Alkali Metal Carbonate Solutions

To characterize the carbonation reaction of calcium sulfate, the interaction between a 0.5 M solution of sodium carbonate and three naturally occurring $CaSO_4$ minerals (i.e., gypsum, bassanite and anhydrite) was initially investigated. Figure 1 provides a summary of the results obtained by in-situ characterization of the reaction progress. Upon addition of solid gypsum to the Na_2CO_3 solution, dissolution began immediately and proceeded quickly, as evidenced by the time-dependent evolution of the Raman peak corresponding to gypsum and the concentrations of aqueous sulfate and calcium ions (Figure 1a–c). The first new solid phase to appear was amorphous calcium carbonate, which was detected in the very first Raman spectra acquired (i.e., at t = 0 min; see Figure S1). The ACC phase rapidly transformed within a few minutes of reaction, yielding vaterite as the sole phase observed by Raman spectroscopy (cf. Figure 1a), as confirmed by the presence of its characteristic double peak at 1090 and 1075 cm^{-1}. During the experiment, the pH of the solution gradually decreased from ~10.7 to ~10.2 after 30 min (cf. Figure 1c), due to the partial consumption of the alkaline carbonate ions via $CaCO_3$ mineralization. In parallel, the conductivity of the solution remained constant during the initial stage of ACC formation and then showed a slight increase upon conversion to vaterite, likely as a consequence of the further release of counterions such as sodium and/or sulfate. Finally, the signal of the calcium ion-selective electrode (Ca-ISE) increased immediately upon addition of gypsum (due to dissolution) and reached a maximum after about 2 min (solubility of ACC), after which it decreased slightly toward the end of the experiment (solubility of vaterite).

Interestingly, the time-dependent behavior was fundamentally different when bassanite (Figure 1d–f) or anhydrite (Figure 1g–i) were used as solid calcium sulfate source. In both cases, the onset

of the dissolution of the added particles was delayed by several minutes, as evidenced by the corresponding Raman spectra (Figure 1d,g), the derived time-dependent profiles of dissolved ion concentrations (Figure 1e,h), as well as the temporal evolution of pH and conductivity (Figure 1f,i). Further characterization of the early stages of the reaction by means of IR spectroscopy (Figure S2) and scanning electron microscopy combined with EDX analysis (Figure S3) shows that ACC was formed after 2 min and persisted for about 3 min before conversion into crystalline polymorphs occurred. These observations indicate that the initial inhibition of mineral dissolution is due to the reaction of carbonate with calcium ions at the surface of the added particles, leading to the formation of a $CaCO_3$ layer that acts as a barrier – a process that might be favored by the higher solubilities of bassanite and anhydrite as compared to gypsum. The signal of the Ca-ISE showed a slight increase in the concentration of dissolved calcium ions immediately after addition of the powders (Figure 1f,i), which was also reflected in the concentration of dissolved sulfate ions (Figure 1e,h). During the initial period of inhibition, no evidence for the formation of ACC could be observed in the Raman spectra (cf. Figure S1), in contrast to the IR data (cf. Figure S2), probably due to the differences in the sensitivity of the two techniques. Once the barrier to dissolution had been overcome (which was longer for bassanite than for anhydrite), carbonation proceeded quickly and yielded calcite instead of vaterite in both cases as evidenced by both IR (cf. Figure S2) and Raman spectra (Figure 1d,g), where the characteristic peak of calcite occurred at 1085 cm^{-1}. As for gypsum as calcium sulfate source, the pH decreased during carbonation while both the calcium potential and the conductivity increased (Figure 1f,i). In parallel, the concentration of dissolved carbonate ions showed a steep decline to reach final levels lower than in the experiment with gypsum (Figure 1,h); in line with the lower final pH values), reflecting the lower solubility of calcite as compared to vaterite.

The results presented above allow us to identify the conditions that favor the formation of vaterite over calcite during the carbonation of calcium sulfate. Calcite tends to be the first, and only, phase to crystallize when an extended induction period occurs before the onset of rapid dissolution of the $CaSO_4$ starting material. More specifically, the direct formation of calcite occurred in solutions with low sulfate and high carbonate concentrations, i.e., at SO_4^{2-}:CO_3^{2-} ratios below 0.2 (cf. Figure 1e,h). In turn, when gypsum was used as calcium sulfate source, rapid dissolution and precipitation of ACC resulted in solution conditions with SO_4^{2-}:CO_3^{2-} ratios higher than 0.2 at the beginning of the reaction and ~0.9 at the time when vaterite crystallization took place (cf. Figure 1b). The observed behavior in terms of phase selection is consistent with previous studies, which reported that SO_4^{2-}:CO_3^{2-} ratios higher than 1 promote the formation and persistence of vaterite [40, 41].

In further experiments, the impact of the type of the alkali counterions on the carbonation reaction of gypsum was investigated by using K_2CO_3 solutions instead of Na_2CO_3. The obtained time-dependent profiles for the evolution of dissolved species and solid phases (Figure S4) were very similar to those discussed above, i.e., ACC was formed immediately and subsequently replaced by vaterite, without major differences in the time of the onset of vaterite crystallization (~7 min) or the corresponding SO_4^{2-}:CO_3^{2-} ratio (~0.8). These findings confirm that the type of the calcium sulfate source used essentially determines the polymorphic outcome of the carbonation reaction.

3.2 | Carbonation of Gypsum in Alkaline Carbon Capture Solutions (ACCS)

In the second part of our work, the methodology described above for alkali metal carbonates was applied in full analogy to carbonate-containing solutions obtained through CO_2 absorption into solutions of alkali metal hydroxides. When using these so-called "alkaline carbon capture solutions" (i.e., ACCS-Na and ACCS-K) with gypsum as calcium sulfate source, the observed general characteristics of the carbonation process were comparable to the experiments performed with Na_2CO_3 and K_2CO_3 solutions, as shown in Figure 2 and Figure S5, respectively. Immediately after the addition of the solid powder, gypsum dissolved and an amorphous precipitate was formed. Within a few minutes, crystallization of vaterite occurred and was completed well before the end of the experiment, with similar timescales for the transformation process (i.e., 5–10 min) in ACCS and alkali metal carbonate solutions of both sodium and potassium (cf. Figure 1, Figure 2; Figures S4, and S5). However, there is one important difference: in ACCS-Na and ACCS-K, vaterite was formed at much lower $SO_4 2^-$:$CO_3 2^-$ ratios (ca. 0.4 and 0.2, respectively) and even lower ratios when the total aqueous carbonate concentration (i.e., $T_{carbonate}$) is considered (ca. 0.2 and 0.1, respectively). Under these conditions, calcite was obtained with bassanite and anhydrite as starting materials in solutions of neat sodium carbonate (cf. Figure 1). This means that in ACCS media, preferential crystallization of vaterite is not driven by the (relative) amount of sulfate ions in solution. Instead, the observed (initial) phase selection can likely be ascribed to two other parameters. First, the pH value during the period of vaterite formation was significantly lower in ACCS-Na (9.2–9.3) and ACCS-K (9.4–9.5) than in solutions of Na_2CO_3 and K_2CO_3 (> 10); indeed, several previous studies have shown that lower levels of pH (7.5–9.7) are favorable for the precipitation of vaterite [16, 42, 43]. The second factor influencing phase selection could be the higher ionic strength (I) in the used ACCS media (> 4 M), which by far exceeds minimum levels of salinity (I > 0.7 M) reported as being beneficial for vaterite formation in the literature [44]. To test the versatility and robustness of our approach to produce vaterite via carbonation of calcium sulfate, we performed additional experiments in which natural gypsum rocks were used after grinding into a powdered material. In ACCS-Na, the observed carbonation behavior was very similar to synthetic gypsum, except for a faster transformation of ACC into vaterite with the natural starting material (ca. 3 instead of 8 min; Figure S6). This shows that the kinetics of the carbonation process depend on various factors that require further investigation.

3.3 | Properties of Vaterite Products

The solid products obtained from carbonation experiments using gypsum as starting material were further characterized in dry state (i.e., ex situ after isolation) by means of powder X-ray diffraction (PXRD), nitrogen sorption, and scanning electron microscopy (SEM). PXRD patterns confirm the presence of vaterite as dominant crystalline phase in all products (Figure S7),

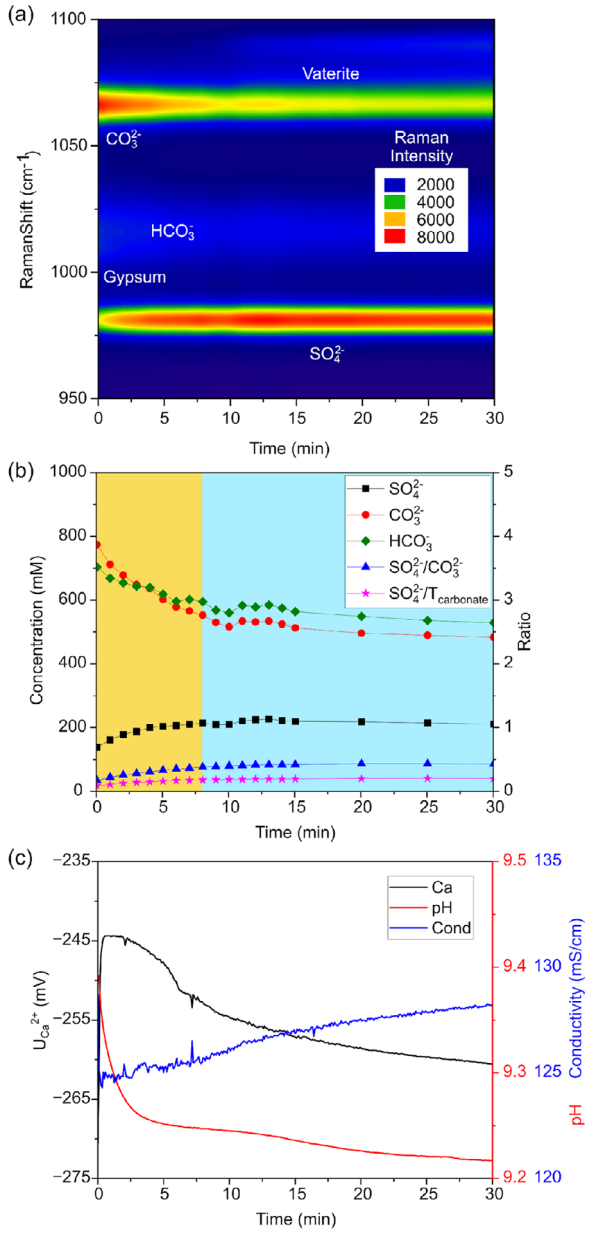

FIGURE 2 | In-situ monitoring of the carbonation of synthetic gypsum in ACCS-Na solution. a) 2D representation of time-dependent Raman spectra acquired during the carbonation process, where characteristic signals of the relevant solid phases and dissolved ions are monitored. b) Temporal evolution of the concentrations of dissolved sulfate, carbonate and bicarbonate ions and the concentration ratios of sulfate to carbonate ions (i.e., SO_4^{2-}/CO_3^{2-}) and sulfate ions to total carbonate content ($T_{carbonate}$, i.e., the sum of CO_3^{2-} and HCO_3^- ions). The presence of ACC and vaterite is indicated by the yellow- and blue-shaded rectangles, respectively. c) Plots of the calcium potential, pH and conductivity as a function of time during the carbonation reaction.

in good agreement with the in-situ Raman measurements, which suggest vaterite fractions higher than 95% after 30 min of reaction based on evaluations according to Equation (1). Quantification with PXRD of the relative amounts of vaterite obtained after carbonation for 30 min using Equation (2) yields values exceeding 98% for all samples except for the product formed from natural gypsum rock, which had a purity of ca. 95%. The remaining 2–5% of crystalline material could be assigned to calcite in all cases, which most likely originates from partial transformation of vaterite during isolation from solution (i.e., filtration and drying) [45]. The results of the PXRD analysis are summarized in Table 2, which also includes findings made for vaterite synthesized by precipitation in two previous studies. We note that the purity of the obtained vaterite indicated by PXRD did not decrease significantly when the carbonation reaction was conducted for longer periods of time (i.e., 60 instead of 30 min), and that all vaterite products remained (meta)stable upon storage in air for at least six months as demonstrated by IR spectroscopy (Figure S8).

One important property for the potential utilization of vaterite in various applications is the specific surface area of the material [13]. The products of the carbonation experiments performed with gypsum in the present work showed S_{BET} values between 9 and 22 m^2/g, whereby the highest and lowest specific surface areas were obtained using synthetic gypsum and natural rock, respectively, in ACCS-Na (Table 2). Among previous studies on the synthesis and characterization of vaterite, only Kim et al. [44] achieved surface areas on comparably high levels. In their work, vaterite was prepared by precipitation in artificial seawater after removal of magnesium from the recipe. In view of practical applications, this appears more complicated than the simple procedure used herein and the reported method did not leverage calcium sulfate as raw material.

The reason for the observed high levels of specific surface area becomes evident from SEM images of the solid products, as shown in Figure 3. On the micron scale (upper panels in Figure 3), particles with rounded shapes were obtained with average sizes (measured for the longest direction) of (4.2 ± 1.3) µm, (2.8 ± 0.8) µm, (4.5 ± 2.0) µm, and (2.0 ± 0.8) µm for synthetic gypsum in 0.5 M Na_2CO_3, 0.5 M K_2CO_3, ACCS-Na and ACCS-K, respectively, and (3.9 ± 0.8) µm for natural gypsum in ACCS-Na. These particles exhibit different degrees of agglomeration and individual morphologies that seem to depend on the type of counterion used: while uniform spheres were formed with potassium, carbonation in the presence of sodium gave various distorted shapes reminiscent of stars or rugby balls – for reasons that remain unknown and certainly require further investigation.

Images with higher magnification (lower panels in Figure 3) reveal that all of these different micron-scale architectures were actually composed of many nanoparticles with similar sizes (<75 nm) and shapes. Such poly- or mesocrystalline texture has been reported for vaterite previously [46, 47] and likely accounts for the high specific surface areas achieved in the present work. Vaterite aggregates comprising the largest nanocrystals were obtained for synthetic gypsum in 0.5 M K_2CO_3 solution ((59.0 ± 14.9) nm), while the smallest primary units were found in products of carbonation with synthetic gypsum in ACCS-Na ((32.0 ± 7.0) nm).

3.4 | Toward Application: Vaterite-Based Cement as Material for Construction

To explore one potential application of the vaterite material obtained through carbonation of calcium sulfate, we used the

TABLE 2 | Vaterite content (X_V) and specific surface area (S_{BET}) of solid products obtained by carbonation of synthetic or natural gypsum in different carbonate-containing solutions. For comparison, values for X_V and S_{BET} reported for vaterite in previous studies are included. The numbers in parentheses represent the experimental error of S_{BET} in %.

	Gypsum source	Reactant solution	X_V (%)	S_{BET} (m^2/g)
This work	Synthetic	0.5 M Na_2CO_3	>98	16 (4)
This work	Synthetic	0.5 M K_2CO_3	>99	20 (4)
This work	Synthetic	ACCS-Na	>99	22 (3)
This work	Synthetic	ACCS-K	>99	16 (5)
This work	Natural	ACCS-Na	~95	9 (7)
Vikulina et al. [29]	None	0.015 M Na_2CO_3 & 0.069 M $CaCl_2$	~100	3.3–7.5
Kim et al. [44]	None	Synthetic seawater without Mg	95.8–100	15.8–27.2

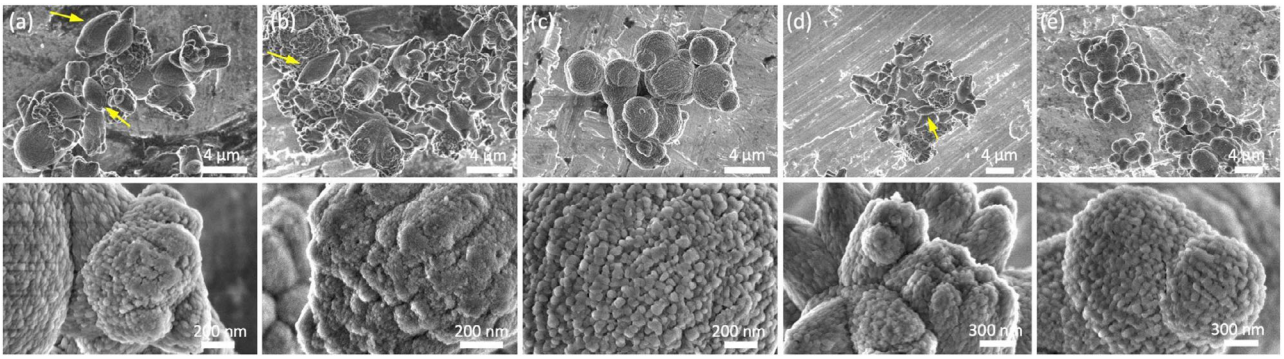

FIGURE 3 | FESEM images of solid products obtained by carbonation of synthetic or natural gypsum in different carbonate-containing solutions, acquired at low (top panels) and high (bottom panels) magnification: a) synthetic gypsum in 0.5 M Na_2CO_3, b) synthetic gypsum in 0.5 M K_2CO_3, c) synthetic gypsum in ACCS-Na, d) synthetic gypsum in ACCS-K, and e) natural gypsum in ACCS-Na. Yellow arrows indicate particles with morphologies reminiscent of rugby balls.

solid product formed with synthetic gypsum in ACCS-Na for a cementation reaction that solely relies on calcium carbonate (and thus completely avoids energy- and CO_2-intensive sintering of conventional clinker), as proposed by Hargis et al. [48]. To this end, the vaterite was mixed with an aqueous solution containing magnesium and strontium chloride at elevated temperature and allowed to react for 24 h. After further curing for another 24 or 48 h, the meanwhile solidified material was characterized by IR spectroscopy, SEM imaging and mechanical testing. Exemplary results are presented in Figure 4. The core mechanism of the cementation process involves the dissolution of metastable vaterite and its subsequent reprecipitation, preferentially in the form of (likewise metastable) aragonite, which is facilitated by the elevated temperature and the presence of magnesium and strontium ions [49]. This polymorphic transformation was shown to be accompanied by a change of particle morphology from spheres (or rounded shapes) to needles, which interlock upon growth and thus generate core strength [48]. In the present work, the successful transformation of vaterite into aragonite upon reaction and curing was confirmed by their characteristic peaks in IR spectra (Figure 4a) [50]. More importantly, the compressive strength of the final solid bodies was comparable to that of ordinary Portland cement (OPC) hydrated with deionized water, whereas OPC mixed with the same solution of magnesium and strontium chloride as used for vaterite exhibited slower strength development (Figure 4b).

To identify the parameters that determine the evolution of compressive strength, we synthesized a series of $CaCO_3$ cements using different reactant solutions and varying the curing temperature. The measured mechanical properties are summarized in Table 3 and compared to the corresponding values of porosity (i.e., specific surface area), phase composition (i.e., fraction of formed aragonite), and particle morphology as derived from SEM images (Figure S9). The data strongly suggests that degree of vaterite-to-aragonite transformation (X_A) achieved after curing is the primary factor enabling high compressive strength. When conversion exceeds 50%, σ values above 8 MPa can be achieved and further increased to 9.3–9.4 MPa in the case of complete transformation. However, such strength levels were only observed for materials consisting of aragonite crystals with sufficiently high aspect ratio (i.e., acicular and/or prismatic instead of equant morphologies). The degree of conversion appears to be mainly influenced by the curing temperature, whereas the composition of the reactant solution plays a less significant role. Finally, the porosity of the material as reflected by the specific surface area does not directly correlate with compressive strength, but it notably decreases with increasing degrees of vaterite-to-aragonite conversion.

Interestingly, the absolute magnitude of compressive strengths determined in the present tests are rather low compared to previous work by Hargis et al., [48] who reported $\sigma \approx 26$ MPa for

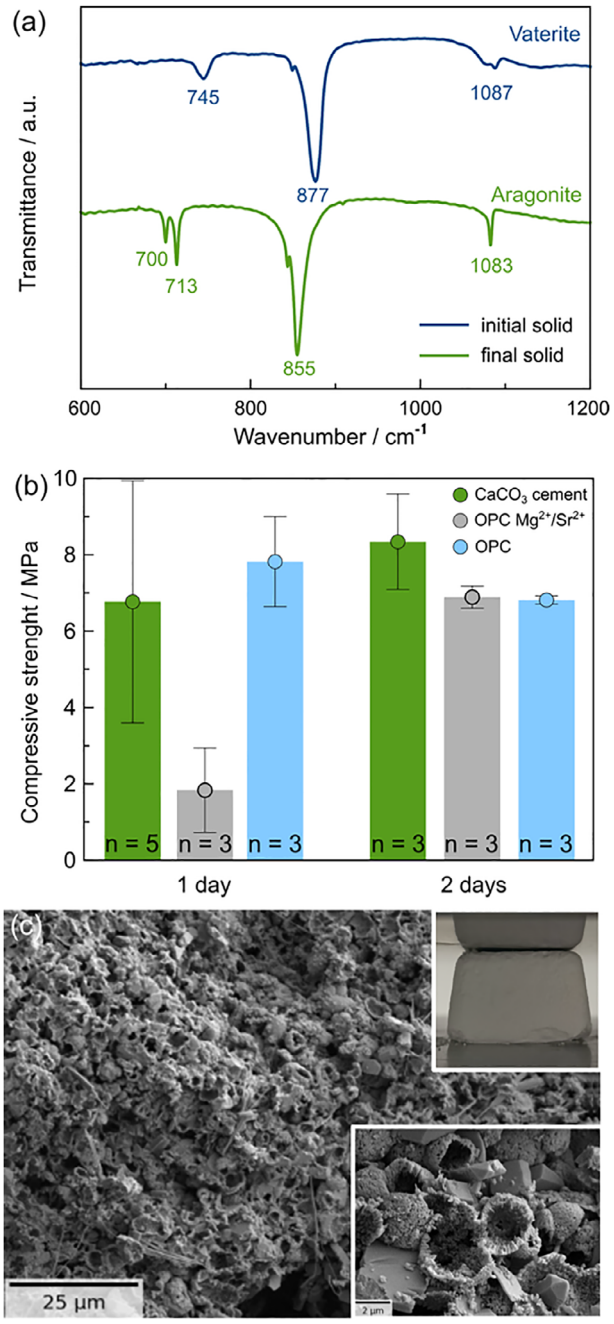

FIGURE 4 | Characterization of solid bodies obtained by cementation of vaterite. a) IR spectra of the used raw material (blue) and the product of the cementation reaction (green), demonstrating the presence of vaterite and aragonite, respectively. b) Compressive strength values determined for vaterite-based cement (green bars) and ordinary Portland cement after curing for 1 and 2 d under the same conditions (i.e., in the presence of Mg^{2+} and Sr^{2+}) and by using deionized water for hydration. The given values represent averages of at least three independent determinations with corresponding standard deviations. Note the large error bar associated with the data after curing the $CaCO_3$ cement for 1 d, which indicates that cementation was not completed at this time in some samples. c) SEM images revealing the microstructure in the core of a hardened $CaCO_3$ cement sample after curing for 2 d. A photograph of the hardened material is shown in the upper inset.

a $CaCO_3$ cement cured in a 0.1 M Mg^{2+}/Sr^{2+} solution at 80°C for 24 h. In turn, significantly lower values ($\sigma \approx 1$ MPa) were found for curing at 40°C. These differences suggest that subtle details of the experimental procedures can strongly impact the properties of the resulting materials and certainly require further investigation to enhance the robustness of the technology. In any case, the observations made in the present work still highlight the potential of vaterite derived from calcium sulfate and carbon dioxide for use as sustainable (and, in the best case, CO_2-negative) building material. In view of such applications, another interesting feature of the cemented calcium carbonate samples is their intrinsic macroporosity, as illustrated by SEM images of the microstructure in their core (cf. Figure 4c; Figure S9): indeed, polymorphic transformation left numerous hollow spheres with diameters of several microns (which do not increase the measured specific surface area substantially). Arguably, the core initially consisted of vaterite (cf. inset in Figure S9a) and the shell was mineralized upon dissolution of vaterite and nearby recrystallization of aragonite (cf. inset in Figure S9d). In our opinion, this unique texture holds promise for a material with acceptable strength and low specific density compared to conventional cements, which could be attractive for lightweight construction concepts. The reason for these interesting characteristics is that the cementation of calcium carbonate described here does not involve a hydration process, as in the case OPC. Thus, the added water is not chemically bound in the forming material but instead evaporates during curing and leads to the observed voids. On the other hand, the SEM images also show that distinct acicular aragonite crystals are only obtained under certain conditions (cf. Figure S9). These structures are comparable to, though less developed than, those reported by Hargis et al. [51]. This rationalizes the relatively low mechanical performance and suggests that significantly higher compressive strength could be achieved with $CaSO_4$-derived vaterite if the conditions of the cementation process are systematically optimized.

3.5 | Implications

The experimental results presented above introduce a new method for the synthesis of pure vaterite that potentially leverages waste and emitted carbon dioxide as raw materials. Thus, the described process could develop into a vital contribution to the global reduction of CO_2 emissions and the required transition of established industrial practices toward more sustainable operations by repurposing waste materials and thus supporting the concepts of a circular economy [9]. A scheme illustrating the envisaged role of calcium sulfate carbonation in a broader and integrated context is shown in Figure 5.

Today, gypsum occurs in abundant amounts as byproduct of different industrial processes. In some cases, like flue gas desulfurization (FGD), the material already finds secondary use and constitutes a essential part of the supply chain for wallboard production. This, however, does not apply for potential calcium sulfate sources that contain critical process-borne contaminants, most notably the so-called "phosphogypsum", which is formed in the production of phosphate fertilizers in global quantities of up to 300 Mt/a. Another major accumulation of gypsum-rich materials results from construction and demolition activities, which leave stockpiles of plasterboard waste on the order of 15

TABLE 3 | Physical properties of $CaCO_3$ cements obtained by mixing vaterite with aqueous solutions containing magnesium and/or strontium chloride and curing at varying temperatures (T) for different times (t). The resulting compressive strength (σ) is compared to the fraction of aragonite (X_A, as determined by IR spectroscopy) formed by polymorphic conversion of vaterite, the specific surface area (S_{BET}) and the dominant habits of aragonite crystals observed by SEM (Figure S9) (n.d.: not determined).

Reactant solution	T [°C]	t [h]	σ [MPa]	Morphology	X_A [%]	S_{BET} [m²/g]
0.1 M Mg^{2+}/Sr^{2+}	80	24	6.2	equant/tabular	100	4.8
0.1 M Mg^{2+}/Sr^{2+}	80	24	8.7	acicular	57	6.7
0.1 M Mg^{2+}/Sr^{2+}	80	48	9.4	acicular	100	5.3
0.1 M Mg^{2+}	80	24	9.3	prismatic/tabular	100	4.3
0.1 M Mg^{2+}	80	24	2.0	prismatic	14	7.3
0.1 M Sr^{2+}	80	24	6.8	equant	48	5.5
0.1 M Mg^{2+}/Sr^{2+}	40	24	8.6	prismatic	57	n.d.
0.1 M Sr^{2+}	40	24	3.8	acicular	19	8.7
0.1 M Mg^{2+}	40	24	1.7	acicular	18	8.8

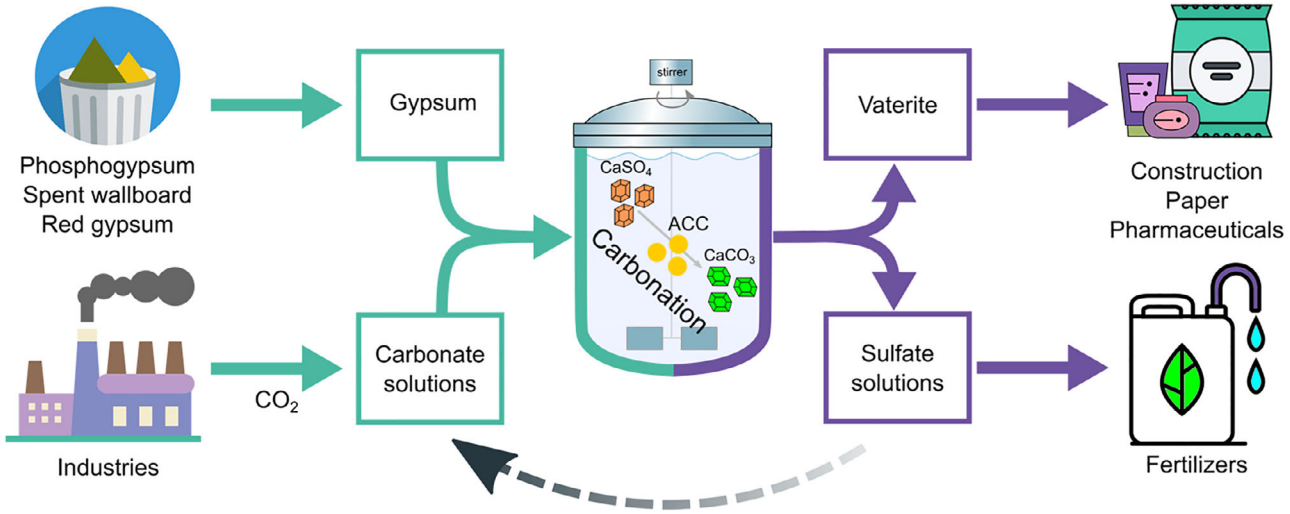

FIGURE 5 | Scheme of processes to obtain value products (vaterite and sulfate solutions) from waste materials (gypsum and carbon dioxide) via carbonation of calcium sulfate. Note that "phosphogypsum" and "red gypsum" are byproducts in the phosphate and titanium oxide industry, respectively.

Mt/a worldwide. At the moment, only a minor fraction of the total gypsum waste (ca. 5% in the European Union) is recovered for reuse. In this context, a process as depicted by Figure 5 could offer an additional pathway to improve gypsum waste management and leverage so far largely untapped resources. In the present study, we have already shown that the proposed method works for both synthetic and natural gypsum (without any pretreatment) as well as with two different types of bases, suggesting a certain degree of broader applicability. However, it is of course necessary to perform further investigations using other calcium sulfate sources such as phosphogypsum or spent wallboards to explore the feasibility of upcycling such waste streams. Indeed, a techno-economic analysis comprising only direct costs (i.e., capital and operational expenditures) and revenues (i.e., product sales) might result in non-profitability. However, the economic viability of the process proposed here should be considered in a wider context with respect to waste management and essentially relies on cost avoidance rather than direct profit. Specifically, the process would mitigate the high costs related to CO_2 capture and storage as well as the financial and environmental burden of gypsum waste disposal. Converting these liabilities into a value product (i.e., vaterite) could thus offer a dual advantage.

At the end of the carbonation of gypsum as conducted in the present work, solid vaterite and a fairly concentrated solution of either sodium or potassium sulfate are obtained. These components must subsequently be separated through filtration or centrifugation, followed by drying of the vaterite material. All these steps may add significant costs and negatively affect sustainability when applied at larger scales. The synthesized calcium carbonate is expected to be of interest to various sectors such as the paper, pharmaceutical and construction industries [10, 11]. Compared to many commercially available grades (which consist of thermodynamically stable calcite), the vaterite product offers two potential advantages: on the one hand, the rounded morphologies of vaterite particles can lead to better dispersion and flowability when used for example as a filler (or partial replacement) of clinker in cement pastes [52]. On the other hand, as a metastable polymorph, vaterite should be considered as

a "reactive" form of calcium carbonate, which may transform into aragonite or calcite under application conditions and could thus add functionality to formulated products. One example in this context is the prototype of a pure calcium carbonate cement, as proposed by Hargis et al. [48, 51]. and confirmed by the tests performed in the present work. However, there is also increasing evidence that the "reactive" character of vaterite may improve the properties of cementitious materials as a functional filler; for instance, calcined clay cements showed faster hydration and higher compressive strength when vaterite was used as supplement instead of calcite [53]. In our opinion, these are only first indications for the benefits of vaterite in calcium carbonate-related applications and more use cases will follow.

Finding a suitable outlet for the second product of the carbonation process (i.e., the aqueous solutions of Na_2SO_4 or K_2SO_4) might be more challenging, mainly because of the rapidly increasing amounts of sodium sulfate waste from the battery industry and the growing difficulties in handling this waste. One possible solution for this problem could be the conversion of Na_2SO_4 into K_2SO_4, which serves as fertilizer in agriculture [54–56]. For the carbonation of gypsum, this would mean that potassium hydroxide should be the base of choice and, most likely, that no evaporation of the liquid product would be needed as K_2SO_4 fertilizers are applied as aqueous solutions. Other potential use scenarios for the sulfate solutions include the precipitation of calcium sulfate hemihydrate (bassanite), [57] which could then be directly employed as hydraulic binder for plasterboards, stuccos, mortars or cements without the need for calcination [58, 59]. Alternatively, gypsum could be crystallized and fed back into the carbonation process in a closed loop (cf. Figure 5). However, in both of these scenarios, a suitable (and sustainable) source of calcium ions would have to be found.

The final point to address in terms of implications is the actual amount of carbon dioxide captured via the carbonation of calcium sulfate. Speciation calculations in PHREEQC [60] predict that for the two alkaline carbon capture solutions used in this work (i.e., ACCS-Na and ACCS-K), ~0.26 kg CO_2 should be sequestered per kg of gypsum in equilibrium and when considering the concurrent precipitation of vaterite. In addition to this direct capture, the later use of vaterite as a functional binder for (partial) replacement of conventional (CO_2-intense) cements would make a further substantial contribution to the overall potential of the technology for carbon management.

4 | Conclusion

In this work, we have shown that high-purity vaterite can be obtained from gypsum powders through a straightforward carbonation reaction in aqueous systems at ambient conditions, which does not require any additives or special precautions. The preferential formation of the metastable polymorph was found to be facilitated by rapid dissolution of calcium sulfate and the intermediate presence of amorphous calcium carbonate, yielding vaterite within less than 10 min. The process was successfully conducted using solutions of different types of alkali metal carbonate as well as the corresponding hydroxides with carbon dioxide as carbonate source. In turn, thermodynamically stable calcite was formed with less hydrated calcium phases (i.e., bassanite and anhydrite) under the same conditions. The vaterite generated by carbonation of gypsum showed interesting properties such as high specific surface area, as a direct consequence of the nanometric size of the constituting primary particles. The potential of the as-prepared vaterite for applications in the construction industry was exemplified in the form of a so-called calcium carbonate cement, which develops into a material with good compressive strength and comparatively low weight via polymorphic transformation into aragonite in water.

The collected data suggests that the carbonation of calcium sulfate could be leveraged as a process to turn abundant gypsum waste into a value product, while at the same time capturing carbon dioxide and utilizing it for construction and other purposes. As the formation of vaterite was shown to occur through dissolution of gypsum and subsequent reprecipitation, contaminants present in the used starting material may be removed during carbonation, such that hitherto untapped resources could become accessible. Although the concept is preliminary and certainly requires further evaluation, our results emphasize the potential of mineralization for carbon capture, storage and utilization, which would contribute to a more sustainable future especially when combined with waste recovery and valorization.

Acknowledgements

C.P. has received funding from the European Union's Horizon 2020 research and innovation programme under the Marie Sklodowska-Curie grant agreement No. 101021894 [CARS-CO2]. A.E.S.V.D., C.P. and P.A.C. acknowledge funding from Ministerio de Ciencia, Innovacion y Universidades under grant PID2023-151099NB-I00. The authors would like to thank Valérie Magnin, Stanislav Jelavic, Rachel Carson and Bruno Lanson for the nitrogen sorption and powder X-ray diffraction measurements, as well as Natasha Acosta and Katja Graf for the preparation and characterization of vaterite-based cements. Sample characterization was performed at the geochemistry-mineralogy platform of ISTerre (UGA, Grenoble, France), which is partially funded by a grant from Labex OSUG@2020 (investissements d'avenir, ANR10-LABX56). The authors further acknowledge support from S.V.G. Repo in curating and hosting the icons used in Figure 5 under the Creative Commons 0 license (CC0).

Funding

Horizon 2020, Marie Sklodowska-Curie (grant agreement No. 101021894 [CARS-CO2]).

Conflicts of Interest

The authors declare no conflict of interest.

Data Availability Statement

The data that support the findings of this study are available from the corresponding author upon reasonable request.

References

1. IEA, CO_2 Emissions in 2022, Paris, France, 2023.

2. S. Solomon, G.-K. Plattner, R. Knutti, and P. Friedlingstein, "Irreversible Climate Change Due to Carbon Dioxide Emissions," *Proceedings of the National Academy of Sciences* 106 (2009): 1704–1709.

3. J. M. Allwood, J. M. Cullen, and R. L. Milford, "Options for Achieving a 50% Cut in Industrial Carbon Emissions by 2050," *Environmental Science & Technology* 44 (2010): 1888–1894.

4. W. J. J. Huijgen and R. N. J. Comans, "Carbonation of Steel Slag for CO 2 Sequestration: Leaching of Products and Reaction Mechanisms," *Environmental Science & Technology* 40 (2006): 2790–2796.

5. A. A. Olajire, "A Review of Mineral Carbonation Technology in Sequestration of CO2," *Journal of Petroleum Science and Engineering* 109 (2013): 364–392.

6. L. Esquivias, V. Morales-Flórez, and A. Santos, "Carbon Dioxide Sequestration by Phosphogypsum Based Procedure," *In Carbon Dioxide Sequestration in Cementitious Construction Materials*. (Woodhead Publishing, 2018).

7. D. Kremer, C. Dertmann, S. Etzold, R. Telle, B. Friedrich, and H. Wotruba, "Ex-situ Mineral Carbonation – A Parameter Study on Carbon Mineralisation in an Autoclave as Part of a Large-scale Utilisation Process," *Journal of CO2 Utilization* 58 (2022): 101928.

8. A. Isah, M. Arif, A. Hassan, M. Mahmoud, and S. Iglauer, "A Systematic Review of Anhydrite-Bearing Reservoirs: EOR Perspective, CO2-Geo-storage and Future Research," *Fuel* 320 (2022): 123942.

9. J. Korhonen, A. Honkasalo, and J. Seppälä, "Circular Economy: the Concept and Its Limitations," *Ecological Economics* 143 (2018): 37–46.

10. Y. Mori, T. Enomae, and A. Isogai, "Preparation of Pure Vaterite by Simple Mechanical Mixing of Two Aqueous Salt Solutions," *Materials Science and Engineering: C* 29 (2009): 1409.

11. D. B. Trushina, T. V. Bukreeva, M. V. Kovalchuk, and M. N. Antipina, "CaCO3 vaterite Microparticles for Biomedical and Personal Care Applications," *Materials Science and Engineering: C* 45 (2014): 644.

12. F. Jin, M. Zhao, M. Xu, and L. Mo, "Maximising the Benefits of Calcium Carbonate in Sustainable Cements: Opportunities and Challenges Associated with Alkaline Waste Carbonation," *npj Materials Sustainability* 2 (2024): 1.

13. F. Liendo, M. Arduino, F. A. Deorsola, and S. Bensaid, "Factors Controlling and Influencing Polymorphism, Morphology and Size of Calcium Carbonate Synthesized through the Carbonation Route: a Review," *Powder Technology* 398 (2022): 117050.

14. Q. Hu, J. Zhang, H. Teng, and U. Becker, "Growth Process and Crystallographic Properties of Ammonia-induced Vaterite," *American Mineralogist* 97 (2012): 1437–1445.

15. R. Chang, D. Choi, M. H. Kim, and Y. Park, "Tuning Crystal Polymorphisms and Structural Investigation of Precipitated Calcium Carbonates for CO 2 Mineralization," *ACS Sustainable Chemistry & Engineering* 5 (2017): 1659–1667.

16. J. M. Williams, D. Zhao, S. Moon, S. Kawashima, A.-H. A. Park, and A. J. Moment, "Stabilization of Pure Vaterite during Carbon Mineralization: Defining Critical Activities, Additive Concentrations, and Gas Flow Conditions for Carbon Utilization," *Crystal Growth & Design* 23 (2023): 8103–8115.

17. X.-H. Guo, S.-H. Yu, and G.-B. Cai, "Crystallization in a Mixture of Solvents by Using a Crystal Modifier: Morphology Control in the Synthesis of Highly Monodisperse CaCO 3 Microspheres," *Angewandte Chemie International Edition* 45 (2006): 3977–3981.

18. K. Song, Y.-N. Jang, W. Kim, et al., "Precipitation of Calcium Carbonate during Direct Aqueous Carbonation of Flue Gas Desulfurization Gypsum," *Chemical Engineering Journal* 213 (2012): 251–258.

19. K. Song, W. Kim, J.-H. Bang, S. Park, and C. W. Jeon, "Polymorphs of Pure Calcium Carbonate Prepared by the Mineral Carbonation of Flue Gas Desulfurization Gypsum," *Materials & Design* 83 (2015): 308–313.

20. Q. Li, Y. Ding, F. Li, B. Xie, and Y. Qian, "Solvothermal Growth of Vaterite in the Presence of Ethylene Glycol, 1,2-propanediol and Glycerin," *Journal of Crystal Growth* 236 (2002): 357–362.

21. D. Liu and M. Z. Yates, "Formation of Rod-Shaped Calcite Crystals by Microemulsion-Based Synthesis," *Langmuir* 22 (2006): 5566–5569.

22. S. Thachepan, M. Li, S. A. Davis, and S. Mann, "Additive-Mediated Crystallization of Complex Calcium Carbonate Superstructures in Reverse Microemulsions," *Chemistry of Materials* 18 (2006): 3557–3561.

23. Y. Baojun, Y. Mengmeng, W. Bainian, F. Xiaoyu, and W. Qiang, "A New Route to Synthesize Calcium Carbonate Microspheres from Phosphogypsum," *Materials Research Express* 6 (2019): 045042.

24. X. Wang, R. Kong, X. Pan, et al., "Role of Ovalbumin in the Stabilization of Metastable Vaterite in Calcium Carbonate Biomineralization," *The Journal of Physical Chemistry B* 113 (2009): 8975–8982.

25. F. Manoli and E. Dalas, "Spontaneous Precipitation of Calcium Carbonate in the Presence of Ethanol, Isopropanol and Diethylene Glycol," *Journal of Crystal Growth* 218 (2000): 359–364.

26. L. Zhang, L.-H. Yue, F. Wang, and Q. Wang, "Divisive Effect of Alcohol−Water Mixed Solvents on Growth Morphology of Calcium Carbonate Crystals," *The Journal of Physical Chemistry B* 112 (2008): 10668–10674.

27. X. Song, H. Liu, J. Wang, Y. Cao, and X. Luo, "A Study of the Effects of NH 4+ on the Fast Precipitation of Vaterite CaCO 3 Formed from Steamed Ammonia Liquid Waste and K 2 CO 3 /Na 2 CO 3," *CrystEngComm* 23 (2021): 4284–4300.

28. G.-T. Zhou, Q.-Z. Yao, S.-Q. Fu, and Y.-B. Guan, "Controlled Crystallization of Unstable Vaterite with Distinct Morphologies and Their Polymorphic Transition to Stable Calcite," *European Journal of Mineralogy* 22 (2010): 259–269.

29. A. Vikulina, J. Webster, D. Voronin, et al., "Mesoporous Additive-free Vaterite CaCO3 Crystals of Untypical Sizes: from Submicron to Giant," *Materials & Design* 197 (2021): 109220.

30. O. Rahmani, R. Junin, M. Tyrer, and R. Mohsin, "Mineral Carbonation of Red Gypsum for CO 2 Sequestration," *Energy & Fuels* 28 (2014): 5953–5958.

31. A. Azdarpour, M. Asadullah, R. Junin, M. Manan, H. Hamidi, and E. Mohammadian, "Direct Carbonation of Red Gypsum to Produce Solid Carbonates," *Fuel Processing Technology* 126 (2014): 429–434.

32. R. Tokpayev, T. Khavaza, Z. Ibraimov, et al., "Phosphogypsum Conversion under Conditions of SC-CO2," *Journal of CO2 Utilization* 63 (2022): 102120.

33. K. Song, Y.-N. Jang, W. Kim, et al., "Factors Affecting the Precipitation of Pure Calcium Carbonate during the Direct Aqueous Carbonation of Flue Gas Desulfurization Gypsum," *Energy* 65 (2014): 527.

34. B. Wang, Z. Pan, Z. Du, H. Cheng, and F. Cheng, "Effect of Impure Components in Flue Gas Desulfurization (FGD) Gypsum on the Generation of Polymorph CaCO3 during Carbonation Reaction," *Journal of Hazardous Materials* 369 (2019): 236–243.

35. G. Montes-Hernandez, J. Weiss, S. Clavier, et al., "Fabrication of Iron-Magnesite under Mild Conditions through Indirect Carbonation of Peridotite and Its Utilization as a Partial Substitute for Cement in Concrete," *Industrial & Engineering Chemistry Research* 64 (2025): 13770–13783.

36. G. Montes-Hernandez and F. Renard, "Time-Resolved in Situ Raman Spectroscopy of the Nucleation and Growth of Siderite, Magnesite, and Calcite and Their Precursors," *Crystal Growth & Design* 16 (2016): 7218–7230.

37. C. G. Kontoyannis and N. V. Vagenas, "Calcium Carbonate Phase Analysis Using XRD and FT-Raman Spectroscopy," *The Analyst* 125 (2000): 251–255.

38. J. Schindelin, I. Arganda-Carreras, E. Frise, et al., "Fiji: an Open-source Platform for Biological-image Analysis," *Nature Methods* 9 (2012): 676–682.

39. A. Singh, S. S. Das, P. R. P. Verma, J. Ruokolainen, K. K. Kesari, and S. K. Singh, "Characterization and Exploration of Placket–Burman-

Designed Porous Calcium Carbonate (Vaterite) Microparticles," *ACS Omega* 8 (2023): 44611.

40. L. Fernández-Díaz, Á. Fernández-González, and M. Prieto, "The Role of Sulfate Groups in Controlling CaCO3 Polymorphism," *Geochimica et Cosmochimica Acta* 74 (2010): 6064–6076.

41. I. Cuesta Mayorga, J. M. Astilleros, and L. Fernández-Díaz, "Precipitation of CaCO3 Polymorphs from Aqueous Solutions: the Role of pH and Sulphate Groups," *Minerals* 9 (2019): 178.

42. I. Udrea, C. Capat, E. A. Olaru, et al., "Vaterite Synthesis via Gas–Liquid Route under Controlled pH Conditions," *Industrial & Engineering Chemistry Research* 51 (2012): 8185–8193.

43. M. Kogo, T. Umegaki, and Y. Kojima, "Effect of pH on Formation of Single-phase Vaterite," *Journal of Crystal Growth* 517 (2019): 35–38.

44. S. Kim, J. Jeon, and M.-J. Kim, "Vaterite Production and Particle Size and Shape Control Using Seawater as an Indirect Carbonation Solvent," *Journal of Environmental Chemical Engineering* 10 (2022): 107296.

45. O. Cherkas, T. Beuvier, F. Zontone, et al., "On the Kinetics of Phase Transformations of Dried Porous Vaterite Particles Immersed in Deionized and Tap Water," *Advanced Powder Technology* 29 (2018): 2872–2880.

46. B. C. Chakoumakos, B. M. Pracheil, R. S. Wood, et al., "Texture Analysis of Polycrystalline Vaterite Spherulites from Lake Sturgeon Otoliths," *Scientific Reports* 9 (2019): 7151.

47. R. Febrida, A. Cahyanto, E. Herda, et al., "Synthesis and Characterization of Porous CaCO3 Vaterite Particles by Simple Solution Method," *Materials* 14 (2021): 4425.

48. C. W. Hargis, I. A. Chen, M. Devenney, M. J. Fernandez, R. J. Gilliam, and R. P. Thatcher, "Calcium Carbonate Cement: a Carbon Capture, Utilization, and Storage (CCUS) Technique," *Materials* 14 (2021): 2709.

49. M. Alkhatib, M. Qutob, S. Alkhatib, and A. Eisenhauer, "Influence of Precipitation Rate and Temperature on the Partitioning of Magnesium and Strontium in Calcite Overgrowths," *Chemical Geology* 599 (2022): 120841.

50. A. G. Xyla and P. G. Koutsoukos, "Quantitative Analysis of Calcium Carbonate Polymorphs by Infrared Spectroscopy," *Journal of the Chemical Society, Faraday Transactions 1: Physical Chemistry in Condensed Phases* 85 (1989): 3165.

51. C. W. Hargis, I. Chen, Y. Wang, H. Maraghechi, R. J. Gilliam, and P. J. M. Monteiro, "Microstructure Development of Calcium Carbonate Cement through Polymorphic Transformations," *Cement and Concrete Composites* 153 (2024): 105715.

52. D. Zhao, J. M. Williams, A.-H. A. Park, and S. Kawashima, "Rheology of Cement Pastes with Calcium Carbonate Polymorphs," *Cement and Concrete Research* 172 (2023): 107214.

53. Y. Li, Y. Li, H. Ma, and J. Li, "The Hydration, Microstructure, and Mechanical Properties of Vaterite Calcined Clay Cement (VC3)," *Cement and Concrete Research* 175 (2024): 107374.

54. P. Huhtanen, S. Ahvenjärvi, and T. Heikkilä, "Effects of Sodium Sulphate and Potassium Chloride Fertilizers on the Nutritive Value of Timothy Grown on Different Soils," *Agricultural and Food Science* 9 (2000): 105–120.

55. A. Ogedengbe, K. Achiobu, S. Scoccimarro, et al., "Valorization of Sodium Sulfate Waste to Potassium Sulfate Fertilizer: Experimental Studies, Process Modeling, and Optimization," *International Journal of Green Energy* 17 (2020): 521–528.

56. H. A. Bahamonde, C. Pimentel, L. A. Lara, V. Bahamonde-Fernández, and V. Fernández, "Foliar Application of Potassium Salts to Olive, with Focus on Accompanying Anions," *Plants* 12 (2023): 472.

57. S. Reigl, A. E. S. Van Driessche, E. Wagner, et al., "Toward More Sustainable Hydraulic Binders: Controlling Calcium Sulfate Phase Selection via Specific Additives," *ACS Sustainable Chemistry & Engineering* 11 (2023): 8450–8461.

58. M. Mishmastnehi, A. E. S. Van Driessche, G. J. Smales, A. Moya, and T. M. Stawski, "Advanced Materials Engineering in Historical Gypsum Plaster Formulations," *Proceedings of the National Academy of Sciences* 120 (2023): 2208836120.

59. S. Reigl, A. E. S. Van Driessche, T. M. Stawski, S. Koltzenburg, W. Kunz, and M. Kellermeier, "Sustainable Pathways for the Synthesis of Calcium Sulfate Hemihydrate," *Angewandte Chemie International Edition* 64 (2025): 202415161.

60. D. L. Parkhurst, *User's guide to PHREEQC: A computer program for speciation, reaction-path, advective-transport, and inverse geochemical calculations*. (US Department of the Interior, US Geological Survey, 1995).

Supporting Information

Additional supporting information can be found online in the Supporting Information section.

Supporting File: adfm74004-sup-0001-SuppMat.pdf.